Derivation of partial pair distribution functions for amorphous FeTb from electron scattering data based on a new concept

1994 J. Phys.: Condens. Matter 6 835

(http://iopscience.iop.org/0953-8984/6/4/004)

J. Phys.: Condens. Matter 6 (1994) 835–848. Printed in the UK

Derivation of partial pair distribution functions for amorphous FeTb from electron scattering data based on a new concept

M Tewes, J Zweck and H Hoffmann
University of Regensburg, Institute of Applied Physics, 93040 Regensburg, Germany

Received 27 August 1993

Abstract. In this work we present pair distribution functions (PDFs) of amorphous $Fe_{1-x}Tb_x$ (x = 0.1–0.5) with a high spatial resolution better than 0.02 nm obtained from electron diffraction experiments. The short-range order of FeTb alloys with up to 32 at.% Tb content is described quantitatively as an arrangement of the known crystalline FeTb phases with various concentrations and structures by superposing PDFs of these structures in the range of the first and second coordination shell up to 0.6 nm. Partial FeFe, FeTb and TbTb radial distribution functions (RDFs) are obtained from this model; coordination numbers and neighbour distances are presented and compared to other authors' results.

1. Introduction

A well established method of structure investigation of amorphous and polycrystalline specimens is the calculation of pair distribution functions (PDFs) from diffraction intensities by means of Fourier inversion. The PDF $g(r) = 4\pi r[\varrho(r) - \varrho_0]$ represents a one-dimensional projection of the autocorrelation function of the structure under investigation. In analogy to crystalline specimens a 'coordination shell' can be defined for amorphous specimens at distances where maxima occur in the PDF. Typically, for amorphous specimens two coordination shells can be found.

The fundamental problem in the interpretation of PDFs of binary alloys such as $Fe_{1-x}Tb_x$ is that the measured total PDF $g(r)$ consists of three partial PDFs $g_{FeFe}(r)$, $g_{FeTb}(r)$ and $g_{TbTb}(r)$ representing FeFe, FeTb and TbTb coordinations. These partial PDFs contribute to the coordination shells in the total PDF weighted according to their atomic concentration and their atomic form factor for the radiation used and cannot be separated from one single diffraction experiment. To overcome this problem, neighbour distances and coordination numbers are often obtained by fitting three Gaussians into the first coordination shell. These Gaussian curves are then assumed to be the three partial PDFs in the range of the first coordination shell. This procedure has been carried out for some rare-earth/transition metal (RE/TM) alloys by several authors (e.g. [1–4]).

However, the visible fine structure of the first coordination shell representing the atomic arrangement may depend strongly on a PDF's spatial resolution. In order to realize a spatial resolution for reliable PDFs, the measurable maximum scattering length k_{max} that can be measured in an experiment has to be as large as possible as has been suggested by numerous authors (e.g.[5–8]. This is an obvious consequence of *Abbe's law of imaging* in an one-dimensional definition.

The short-range order of FeTb or related RE/TM alloys has been interpreted in most cases with 'dense random packing' models (see [9] for an overview). In this work a different

0953-8984/94/040835+14$07.50

description is given in terms of a structure model that describes the amorphous structure as a simultaneous existence of several crystal-like types of short-range order. From this model, which seems to give a more appropriate description especially for the atomic arrangement of Fe-rich alloys, partial FeFe, FeTb and TbTb coordinations are calculated and discussed.

2. Experimental procedure

2.1. Preparation and measurements

All the FeTb alloys investigated were prepared as thin films by RF sputtering in Ar atmosphere. The sputtering power was 200 W, the Ar partial pressure 10^{-2} hPa, the initial pressure less than 10^{-7} hPa. The films were deposited on water-cooled glass substrates. The sputtering rate was 0.4 nm s^{-1}. Two film thicknesses—10 nm and 50 nm—of each composition were sputtered, mainly to investigate incoherent electron scattering contributions depending on the film thickness. To prevent oxidation the films were covered with an Al under- and overlayer of 5 nm thickness, thus forming a sandwich layer of Al/FeTb/Al. The Al cover was found to be very stable and to reliably prevent the oxidation of the films.

The film compositions were determined by Auger electron spectroscopy (AES) and by energy dispersive x-ray (EDX) spectroscopy. Using a parallel electron energy-loss spectrometer (PEELS), it was also possible to check qualitatively that no oxidation had occured in the films under investigation. In all films 1–2 at.% Ar was found from the sputtering process.

The structure of the films was investigated with electron diffraction measurements in a conventional transmission electron microscope (TEM Philips CM 30) in diffraction mode with 300 keV electrons. The camera length L was used to calculate the scattering angle

$$2\Theta = \tan^{-1}\frac{D}{L} \tag{1}$$

with D the distance from central (unscattered) spot to the scattered electron intensity. Θ was used to calculate the scattering length k, which is defined as

$$k = \frac{4\pi \sin\Theta}{\lambda} \tag{2}$$

with λ = 1.97 pm (de Broglie wavelength of 300 keV electrons).

The diffraction patterns were recorded with a CCD slow-scan camera connected to the electron microscope. In this case, no normalization procedure had to be performed besides the standard dark-current subtraction and gain-variation normalization due to the very good linear response of the CCD signal to electron intensities. A very good signal-to-noise ratio up to high scattering lengths – where the scattered intensities are very weak – was reached by using longer integration times in this area. This is shown in figure 1 for two independently measured scattering intensities of a crystalline $Fe_{95}Tb_5$ specimen with BCC Fe structure. Each intensity represents a superposition of four measurements, which is the standard procedure used for all measurements in this work. Besides a scaling to the integration time used no additional data processing such as smoothing was performed.

As a second independent method micrographs were taken from the diffraction patterns, their local optical density was obtained from densitometer traces and converted into electron intensities with a normalization procedure as described in [10]. Here also series with increasing integration times were measured. No differences were found between the results of both methods.

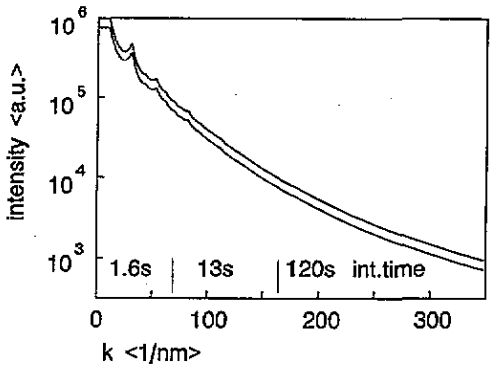

Figure 1. Scattering intensities $I_{exp}(k)$ from two independent measurements for a crystalline $Fe_{95}Tb_5$ film. The intensity is shown on a logarithmic scale, for ease of comparison the upper curve has been shifted. The intervals where different integration times are used are indicated at the k-axes.

2.2. *PDF calculation and interpretation*

The well known algorithm to calculate PDFs $g(r)$ from the measured scattering intensity $I_{exp}(k)$ has been described in detail, for example in [11]. We use the same procedure as in [10], where a Lorch function $M(k)$ [12] is used to avoid ripples in the PDF caused by the upper integration limit k_{max} in (3):

$$g(r) := 4\pi r\left[\varrho(r) - \varrho_0\right] = \frac{2}{\pi}\int_0^{k_{max}} ki(k)\sin(kr)M(k)\,\mathrm{d}k \tag{3}$$

with $i(k)$ the so-called reduced interference function defined as

$$i(k) = \frac{I_{exp}(k)}{N|f(k)|^2} - 1 \tag{4}$$

where $|f(k)|^2$ is the atomic form factor of the specimen and N is a scaling factor, so that $i(k)$ represents only the structure-sensitive part of $I_{exp}(k)$. For alloys, $|f(k)|^2$ is the sum of the atomic form factors of the elements weighted to their atomic concentrations. The Lorch function is defined as

$$M(k) = \begin{cases} \sin(\pi k/k_{max})/(\pi k/k_{max}) & \text{for } 0 \leqslant k \leqslant k_{max} \\ 0 & \text{otherwise.} \end{cases} \tag{5}$$

Coordination numbers Z in an interval r_1–r_2 in real space are calculated as the integral

$$Z = \int_{r_1}^{r_2} G(r)\,\mathrm{d}r \tag{6}$$

with $G(r)$ the so-called radial distribution function (RDF) defined as

$$G(r) = rg(r) + 4\pi r^2\varrho_0 \tag{7}$$

For a detailed and reliable PDF and RDF interpretation the error limits of the procedure described must be checked very carefully. In this work attention has been paid especially to

(1) the PDFs' spatial resolution, (2) the accuracy of the PDFs' amplitudes and (3) a possible contribution of the Al coverage of the investigated films.

(1) As mentioned in the introduction, it is well known that the spatial resolution Δ of a PDF is limited by the maximum measured scattering length k_{max} by

$$\Delta = \frac{2\pi}{k_{max}}. \tag{8}$$

Δ is the limiting factor for the separation of neighbour distances. Therefore, even for amorphous specimens it is necessary to extend the scattering vector up to high values between 300 and 400 nm^{-1} to improve the resolution in real space up to 0.02 nm (see [8] for a detailed discussion). Especially for Fe-rich FeTb alloys with Tb content between 10 and 20 at.% Tb where the transformation from crystalline to amorphous state is observed, a resolution of 0.02 *nm* is necessary to separate neighbour distances that exist in BCC Fe and to investigate the FeTb coordination, which has been assumed to be quite complicated for example for $Fe_{80}Tb_{20}$ [13]. Therefore, we have measured scattering intensities up to a k_{max} of about 350 nm^{-1}. In figure 2(a) the functions $ki(k)M(k)$ calculated from the intensities in figure 1 are shown together with the difference. As can be seen, for the polycrystalline specimen used as a test structure significant peaks can be seen at least up to 250 nm^{-1}. To prove that real information in $i(k)$ can be measured up to the maximum measured scattering length, the standard deviations of the three curves were calculated. For the difference of the two measurements, which represents the pure noise without structure information, the standard deviation is given by twice the averaged height of the noise signal. For the $ki(k)M(k)$ curves, which oscillate around zero, the standard deviation is given by the averaged signal height. The calculation was performed independently for three intervals: The standard deviation of the $ki(k)M(k)$ curves was found to be 3.56 nm^{-1} between 0 and 100 nm^{-1}, 0.70 nm^{-1} between 100 and 200 nm^{-1} and 0.37 nm^{-1} between 200 and 350 nm^{-1}. The standard deviations of the difference are 0.094 nm^{-1}, 0.090 nm^{-1} and 0.079 nm^{-1}, respectively. This means that there is real information in the scattered intensity over the whole range measured, with a averaged signal-to-noise ratio of roughly 80:1 in the first interval, 15:1 in the second and still 10:1 in the third.

(2) The measured intensity $I_{exp}(k)$ in electron diffraction experiments has contributions not only from the coherent scattering from the specimen. Other contributions are caused by *inelastic* scattering processes in the specimen and by multiple-scattering effects [14]. This causes a change of the peak-to-background ratio, where the coherent Bragg-scattered intensity decreases and the incoherent background increases. Moreover, the multiple-scattering effects influence the shape of the background, which causes long-range disturbance in $i(k)$ and therefore ripples at small distances ($\leqslant$ 0.15 nm) in $g(r)$. To study these contributions we used different film thicknesses of the same specimen as suggested in [14]. To correct these effects quantitatively we used a polycrystalline, textureless 50 nm thick $Fe_{95}Tb_5$ specimen with BCC Fe structure as a reference, where the background curve can be measured directly as suggested in [11]. This method has been chosen because so far no first-principles correction method has been introduced especially for the correction of multiple scattering effects in $I_{exp}(k)$.

An additional correction, which is necessary because of the limitations of the apparatus, is the removal of a damping term the PDF is unavoidably multiplied due to a convolution of $I_{exp}(k)$ with the finite electron-source size, the imaging conditions in the electron microscope and the finite resolution of the camera system used for registration.

These correction procedures limit the accuracy of PDF amplitudes (and therefore coordination numbers) to a systematic error of 10–20 %, while the statistical error is much

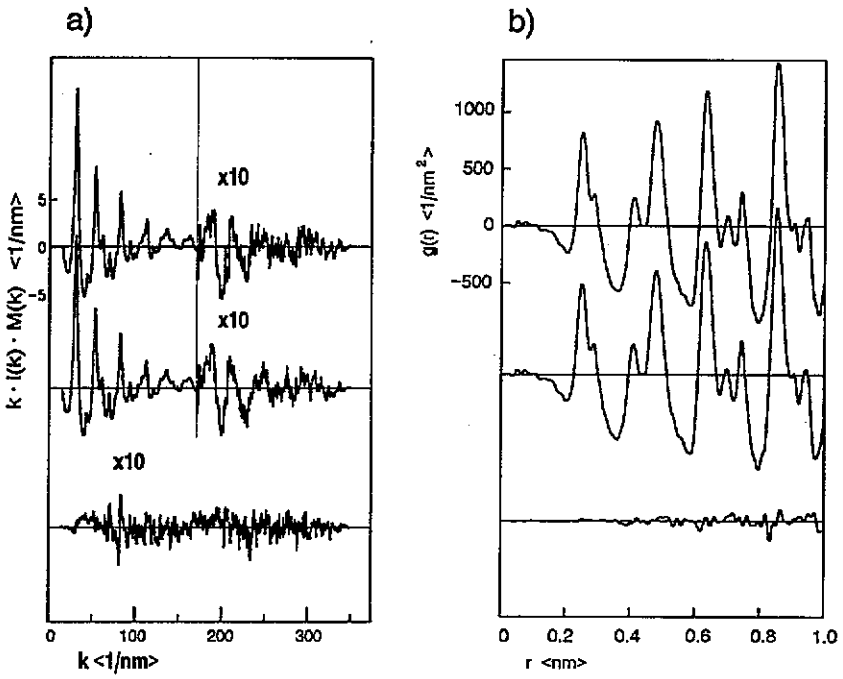

Figure 2. (a) Calculated functions $ki(k)M(k)$ according to equations (4) and (5) from the measured intensities in figure 1 (top and middle) and the difference between the two (bottom). Note that the scale of the y-axis is changed for the top and middle curves at 170 nm^{-1}, and for the bottom curve as a whole, by a factor of ten. (b) PDFs calculated from the curves in (a) according to equation (3) (top and middle) and the difference (bottom). The same scale is used for all three curves.

smaller: in figure 2(b) the PDFs calculated from the intensity curves of figure 2(a) are shown together with their difference. The absolute difference, which is roughly twice the statistical error, is smaller than $\pm$ 15 nm^{-2} in the range of the first coordination shell and smaller than $\pm$ 30 nm^{-2} in the range of the second coordination shell. The increase of the difference is caused by the removal of the damping term. This means that the statistical error caused by uncertainties of the measured intensities is smaller than 2%. This error is shown in figure 3 as error bars for the first, second and third coordination shells for the PDFs of all specimens presented there.

The *positions* of the maxima in $g(r)$ are nearly independent of these effects[14]. Besides peak broadening, the error in r in real space is about the same as the error in k in reciprocal space which is very small ($\leqslant 0.1\%$).

(3) Although inelastic- and multiple scattering contributions in $I_{exp}(k)$ are much larger for the 50 nm thick FeTb films than for the 10 nm films, only the former are used to calculate PDFs because no correction for an Al contribution has to be made: due to a smaller number density and smaller atomic form factor the theoretically scattered intensity ratio Al:FeTb is only 1:20 for the film thickness ratio of 1:5. In an experiment the contribution is even smaller, because weaker Bragg peaks of the Al coverage at larger k-values are not registered due to the finite signal-to-noise ratio of roughly 15:1 above 100 nm^{-1}. Therefore, only a very weak and smeared-out Al contribution in the FeTb PDFs has to be expected. This can be seen directly in figure 3: the long range order of Al crystallites would be seen as significant peaks in PDFs of amorphous FeTb specimens such as $Fe_{82}Tb_{18}$ at larger distances,

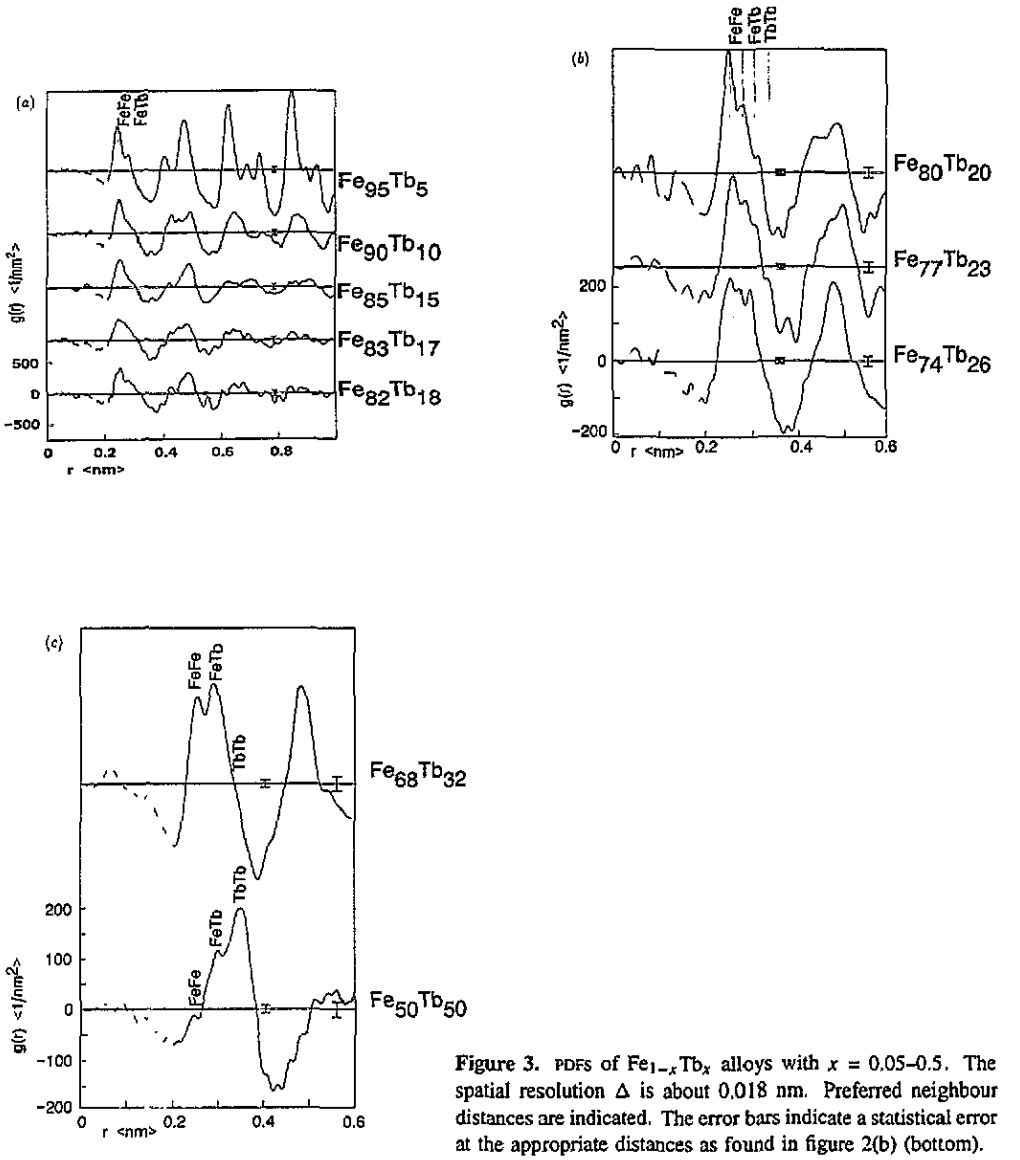

Figure 3. PDFs of $Fe_{1-x}Tb_x$ alloys with x = 0.05–0.5. The spatial resolution Δ is about 0.018 nm. Preferred neighbour distances are indicated. The error bars indicate a statistical error at the appropriate distances as found in figure 2(b) (bottom).

but in fact only small ripples can be seen beyond 0.7 nm.

2.3. Results

Well known basic structural features of amorphous FeTb alloys can be seen in the PDFs presented in figure 3: an FeFe next-neighbour distance of (0.255± 0.005) nm can be found over the whole concentration range. A decrease of the short-range order down to two coordination shells can be observed with increasing Tb content from 10 to 20 at.% Tb and an FeTb neighbour distance in the PDFs appears at about 0.307 nm. Beside these well known features of the first coordination shell, significant differences of the fine structure can now

be observed with increasing Tb content of the alloys due to the high spatial resolution of the PDFs, as follows.

(1) Tb content 10–18 at.% (first panel of figure 3): the polycrystalline long range order as in BCC Fe is destroyed. In the first coordination shell the second BCC FeFe neighbour distance at 0.29 nm can no longer be separated. This is due to a broader range of FeFe next-neighbour distances in the less ordered specimens. Also an FeTb coordination with increasing Tb content can be seen. The atomic distances observed become less localized with increasing Tb content, indicating the transition from a crystalline to an amorphous state. A TbTb coordination cannot be observed because of the small weighting factor in this composition range (less than 5%).

(2) Tb content 20–26 at.% (second panel of figure 3): in this range a substructure in the first coordination shell becomes more pronounced, showing four submaxima for $Fe_{77}Tb_{23}$ or three submaxima and an additional shoulder for $Fe_{80}Tb_{20}$ and $Fe_{74}Tb_{26}$. This fine structure is significant for the three specimens in this composition range. It is significantly larger than a possible statistical or termination error as indicated by the error bars. Therefore, the structure cannot easily be interpreted with the idea of *one* fundamental distance each for FeFe, FeTb and TbTb coordination, respectively. The reason why this fine structure has not been found in the few other works on Fe-rich FeTb alloys [2, 3] can be found from the fact that in our experiments a higher spatial resolution is achieved and that electron diffraction is more sensitive to the partial FeFe coordination than x-ray diffraction. This is due to a higher ratio of the atomic form amplitudes $f_{Fe} : f_{Tb}$ for electron compared to x-ray scattering [15].

(3) Tb content 32–50 at.% (third panel of figure 3): three subpeaks appear in the first coordination shell of the PDF, interpreted as FeFe, FeTb and TbTb distances. This result has been reported by other groups for $Fe_{67}Tb_{33}$ and more Tb-rich alloys [1, 3, 16, 17]. An interpretation as a random packing of hard spheres, where the atomic distances are given according to the Goldschmidt diameters of the atoms, seems to be possible in this case as has been often discussed [9]. However, this model cannot explain the structures shown in the first two panels of figure 3.

3. A structure model for amorphous FeTb alloys

3.1. Model calculations

To describe the fine structure discussed above quantitatively we fit a linear combination of the six crystalline structures of the FeTb phase diagram (BCC Fe, the rhombohedral phase of $Fe_{17}Tb_2$, Fe_3Tb, $Fe_{23}Tb_6$, Fe_2Tb and HCP Tb) [18] to the first coordination shell in the PDFs. The physical meaning of this fit is to describe the short-range order of binary non-crystalline atomic systems as a simultaneous existence of associations corresponding to crystalline structures with various concentrations and structures. The general idea has been developed from thermodynamical considerations by Aptekar [19].

It should be mentioned that this model is completely different to a so-called 'quasicrystalline' (QC) model, which assumes the short-range order of the amorphous state to be identical to that of *one* crystalline structure of similiar stoichiometry. Therefore, we want to call our model a 'multicrystalline' (MC) model, which is more similiar to the model of 'random packing of molecular units' (RPMU) introduced by Gaskell [20] to describe the short-range order of metal/metalloid alloys.

The QC model has been discussed in recent years for RE/TM alloys without success [1, 15, 16]. In particular, for amorphous Fe_2Tb and Fe_2Gd it has been found that the short-range order of the crystalline Laves phase ($MgCu_2$ structure type) differs both in neighbour

distances and coordination numbers from the short-range order of the amorphous phase with the same composition.

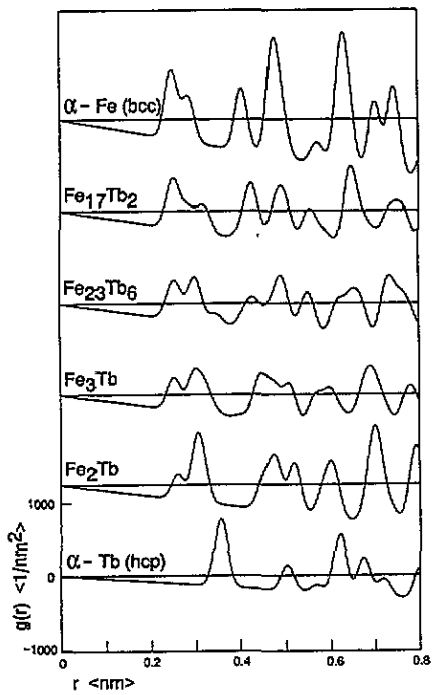

Figure 4. Calculated PDFs of crystalline Fe, Tb and FeTb structures with a resolution Δ of 0.02 nm as used for the MC model.

The calculated PDFs of all the crystalline structures used are shown in figure 4; next-neighbour distances and coordination numbers of the crystalline structures are summarized in table 1. A linear combination of these calculated PDFs of the crystalline structures were fitted to the first coordination shell of the experimentally obtained PDFs. The full widths at half maximum of the crystalline PDFs were varied in a range of 0.015 nm (experimental resolution) to 0.04 nm. The best results were obtained with widths of about 0.025 nm. This is a larger width than expected for *crystalline* structures and is interpreted as a disturbed crystalline order in the range of the first coordination shell of the amorphous specimens.

Table 1. Neighbour distances and coordination numbers of crystalline Fe, FeTb and Tb structures averaged according to a PDF resolution Δ of 0.02 nm as in figure 4.

Crystalline structure	FeFe		FeTb		TbTb	
	Coordination	Distance (nm)	Coordination	Distance (nm)	Coordination	Distance (nm)
Fe	14	0.249 0.285	—	—	—	—
$Fe_{17}Tb_2$	10.4	0.252 0.300	2.7	0.290 0.321	1.0	0.415
$Fe_{23}Tb_6$	9.1	0.254	3.3	0.301	3.9	0.344
Fe_3Tb	7.4	0.252	4.7	0.302	3.4	0.328
Fe_2Tb	6	0.259	6	0.304	6.6	0.318
Tb	—	—	—	—	12	0.356

Having found the distribution of the crystalline structures in the amorphous alloys, partial RDFs were calculated for the amorphous FeTb alloys by adding the correctly weighted calculated partial RDFs of the crystalline structures. Finally, from these RDFs partial

coordination numbers, Z_{ij}, according to equation (6), and neighbour distances, r_{ij}, are obtained.

Table 2. Contributions C_k of crystalline FeTb structures in PDFs of amorphous FeTb alloys in %, normalized to 100%.

Amorphous alloy	C_{Fe}	$C_{Fe_{17}Tb_2}$	$C_{Fe_{23}Tb_6}$	C_{Fe_3Tb}	C_{Fe_2Tb}	C_{Tb}
$Fe_{90}Tb_{10}$	68	22	—	—	7	3
$Fe_{85}Tb_{15}$	65	18	—	—	6	11
$Fe_{83}Tb_{17}$	54	28	—	3	7	8
$Fe_{82}Tb_{18}$	28	41	22	2	4	3
$Fe_{80}Tb_{20}$	28	28	31	1	4	8
$Fe_{77}Tb_{23}$	27	18	28	7	10	10
$Fe_{74}Tb_{26}$	17	18	46	8	—	11
$Fe_{68}Tb_{32}$	11	10	29	28	9	13
$Fe_{50}Tb_{50}$	4	—	—	—	36	60

Table 3. Fit parameters: Fe content c_{Fe} and mean deviations σ_1 and σ_2 in the first) and second coordination shells respectively.

Amorphous alloy	c_{Fe} (at.%)	σ_2 (%)	σ_2 (%)
$Fe_{90}Tb_{10}$	92	2.3	11.4
$Fe_{85}Tb_{15}$	85	3.0	7.3
$Fe_{83}Tb_{17}$	86	3.7	9.0
$Fe_{82}Tb_{18}$	86	1.9	6.8
$Fe_{80}Tb_{20}$	81	1.5	6.1
$Fe_{77}Tb_{23}$	77	3.6	6.6
$Fe_{74}Tb_{26}$	76	2.5	7.4
$Fe_{68}Tb_{32}$	70	2.8	5.9
$Fe_{50}Tb_{50}$	28	5.3	67.4

In table 2 a summary of the results for the FeTb alloys is given. In table 3 several parameters are listed, which are defined to check the reliability of the results as follows.

(1) The mean deviation σ_1 is defined as the average deviation between measured and fitted PDFs within the fit interval normalized to the PDF's amplitude. It would be zero for an ideal fit.

(2) From the results in table 2 the Fe content c_{Fe} of the amorphous FeTb alloys can be calculated. This average composition of the different local stoichiometries has to be equal to the macroscopically measurable composition. This is an important test for the physical significance of our model. An absolute error of about 5 at.% is assumed.

(3) If there are crystalline-type bondings in the amorphous specimens as predicted by the MC model, the fit performed on the first coordination shell should describe some significant details of the *second* coordination shell as well. An additional disturbance as normally assumed for amorphous structures can be taken into account by smoothing the second coordination shell in the fitted PDFs. Results for some FeTb alloys can be seen in figure 5. As can be seen, the only structure where the fit does not describe the limits and amplitude of the second coordination shell accurately is $Fe_{50}Tb_{50}$. Also the calculated Fe content for this fit is wrong. Possible reasons for this result will be discussed in detail below. The mean deviation for the second coordination shell σ_2 between measured and fitted PDFs is also given in table 3.

Summarizing, it can be stated that for the Fe-rich FeTb alloys there is a strong evidence for the MC model: the mean deviation between measured and fitted PDFs within the fitting

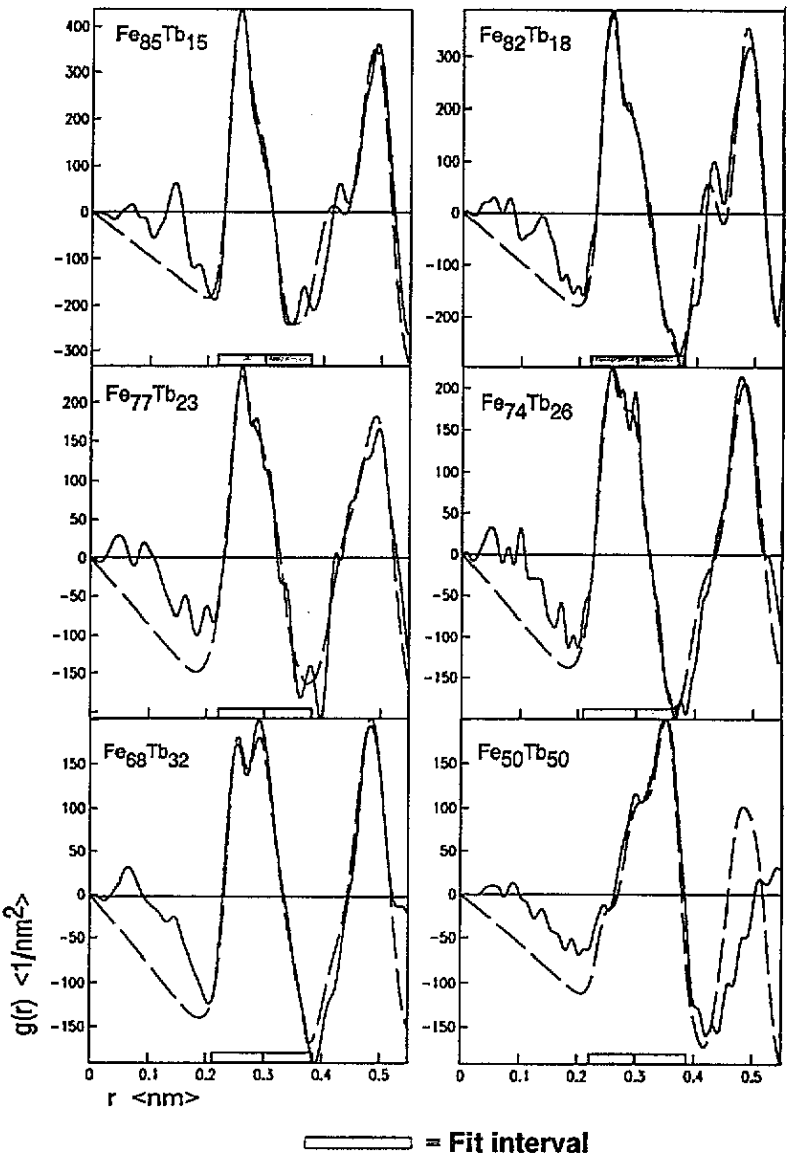

Figure 5. PDFs of amorphous FeTb alloys (——) with fitted PDFs (- - - -).

limits (first coordination shell) is about 2.7%, for the second coordination shell it is about 7.5% and the macroscopic Fe content is reproduced within error limits of 4 at.%.

It should be mentioned here that for Gaussians fitted to the first coordination shell to describe the short-range order, the check for validity of this procedure that can be made is the quality of the fit within the fitting limits only. The criteria used to check our model are much stronger. A physically meaningful interpretation of the fit results seems to be possible.

3.2. Distribution of the crystalline FeTb structures in amorphous FeTb

Our MC model gives a complicated correlation between the Tb content and the distributions

of crystalline FeTb structures in the amorphous alloys: in no alloy is the crystalline phase that contributes most to the fit that with the composition closest to that of the amorphous alloy, as a QC model would suggest. It seems that there is a small 'segregation' of about 5–10% Tb that can be found in every FeTb alloy, while the alloys' short-range order is dominated by a more Fe-rich crystalline structure (BCC Fe up to 17 at.% Tb in the amorphous alloy, $Fe_{17}Tb_2$ for $Fe_{82}Tb_{18}$, $Fe_{23}Tb_6$ for $Fe_{80}Tb_{20}$ up to $Fe_{68}Tb_{32}$).

For the $Fe_{50}Tb_{50}$ alloy this description is not valid. HCP-Tb-like ordered regions seem to dominate this alloy. A complete description of this structure in terms of the MC model does not seem to be possible. It should be mentioned that the model seems to give good results exactly in the composition range of the *amorphous* FeTb alloys where *crystalline* FeTb structures exist.

3.3. Coordination numbers and neighbour distances of amorphous FeTb

The partial RDFs calculated from the values of table 2 for the amorphous alloys are shown in figure 6, the results are summarized in table 4. The weighting factors for the partial TbTb RDFs are too small for the alloys up to $Fe_{83}Tb_{17}$ to calculate reliable TbTb coordination numbers. An error of ± 10% is reliable for the coordination numbers. For the neighbour distances an error of ± 1% can be assumed.

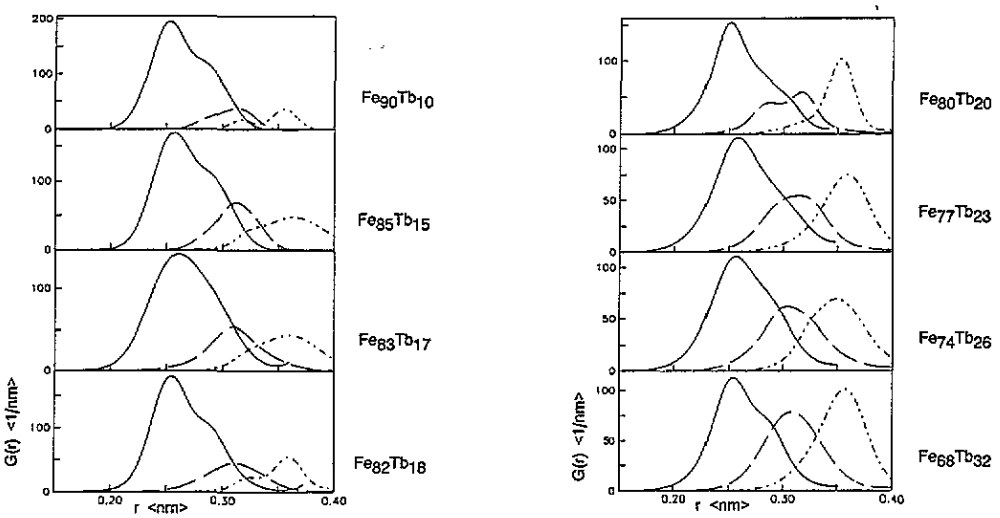

Figure 6. Partial RDFs of the amorphous FeTb alloys calculated from fit results. (——, FeFe; - - - -, FeTb; and — · —, TbTb).

Additionally, in table 4 coordination numbers and neighbour distances of $Fe_{68}Tb_{32}$ and $Fe_{50}Tb_{50}$ are given that have been obtained by fitting three Gaussians within the limits of the first coordination shell. For $Fe_{50}Tb_{50}$ this method seems plausible, as discussed above, for $Fe_{68}Tb_{32}$ it is interesting to compare the two results.

Table 5 gives results presented in other publications for alloys $Fe_{80}Tb_{20}$ and $Fe_{67}Tb_{33}$ or similar. As can be seen, coordination numbers differ for different authors, while neighbour distances are mainly the same. As discussed, coordination numbers are very sensitive to normalization errors, methods of fitting and also to the RDFs' spatial resolution Δ [3]. This is as likely a reason for the differences as a real structural difference due to different specimen preparation.

Table 4. Neighbour distances and coordination numbers of FeTb alloys from fit results in table 2 (* from fitting three Gaussians) and the surplus of Tb atoms around Fe compared to statistic distribution in the next-neighbour shell.

Amorphous alloy	FeFe		FeTb		Surplus of FeTb	TbTb	
	Coordination	Distance (nm)	Coordination	Distance (nm)	Coordination	Coordination	Distance (nm)
$Fe_{90}Tb_{10}$	11.9	0.252	1.8	0.313	+ 0.4	—	—
$Fe_{85}Tb_{15}$	11.0	0.256	3.3	0.311	+ 1.2	—	—
$Fe_{83}Tb_{17}$	10.6	0.260	3.1	0.309	+ 0.8	3.3	0.360
$Fe_{82}Tb_{18}$	9.7	0.254	2.6	0.310	+ 0.7	3.0	0.360
$Fe_{80}Tb_{20}$	8.1	0.250	2.9	0.288 0.317	+ 0.7	3.3	0.353
$Fe_{77}Tb_{23}$	7.5	0.258	3.6	0.315	+ 1.0	4.1	0.359
$Fe_{74}Tb_{26}$	6.8	0.256	3.8	0.304	+ 1.0	4.0	0.349
$Fe_{68}Tb_{32}$	6.0	0.254	4.4	0.308	+ 1.1	4.9	0.357
	5.0	0.254	5.0	0.305	+ 1.8	5.0	0.348*
$Fe_{50}Tb_{50}$	4.8	0.260	3.8	0.306	−0.5	8.4	0.353*

Table 5. Neighbour distances and coordination numbers of FeTb alloys from various authors.

Amorphous alloy	FeFe		FeTb		TbTb		
	coordination	Distance (nm)	coordination	Distance (nm)	coordination	Distance (nm)	Reference
$Fe_{81}Tb_{19}$	6.8	0.252	2.9	0.302	3.4	0.341	[4]
$Fe_{80}Tb_{20}$	7.1	0.250	3.4	0.303	3.6	0.347	[3]
$Fe_{79}Tb_{21}$	7.0	0.259	—	0.306	6.9	0.349	[2]
$Fe_{71}Tb_{29}$	5.4	0.249	4.5	0.303	3.1	0.341	[3]
$Fe_{67}Tb_{33}$	6.3	0.254	3.3	0.304	6.0	0.347	[1]
$Fe_{67}Tb_{33}$	6.4	0.255	5.1	0.320	6.3	0.340	[16]
$Fe_{63}Tb_{37}$	4.2	0.249	4.9	0.300	5.4	0.343	[3]

The positions of the main maxima of the partial FeFe and FeTb RDFs (table 4) are in good agreement with the next neighbour distances found by other authors. They are close to the sum of the Goldschmidt radii of Fe and Tb.

In figure 6, the partial FeFe RDFs show over the whole composition range a more or less pronounced shoulder at about 0.29 nm, which gives the first coordination shell a shape similiar to that of BCC Fe. This result is found also for partial FeFe RDFs where the proportion of the BCC Fe RDF is only 10–20%, as for $Fe_{74}Tb_{26}$ or $Fe_{68}Tb_{32}$. This means that a BCC Fe-like shape of the first FeFe coordination can also be found from a superposition of the partial FeFe RDFs of the crystalline FeTb structures.

The partial FeTb RDFs are also of non-Gaussian shape in the range of the first coordination shell. Here a shoulder at smaller distances than the main maximum can be seen; for the partial FeTb RDF of $Fe_{80}Tb_{20}$ a real submaximum at 0.29 nm shows up.

The partial TbTb RDFs are dominated by the HCP Tb part, but show also contributions of the TbTb coordinations of the crystalline FeTb structures at smaller neighbour distances. The maximum for the TbTb neighbour distance is about 0.355 nm, slightly larger than the more often reported 0.34–0.35 nm.

Summarizing, the atomic arrangement around an Fe atom consists of Fe atoms at mainly two distances at about 0.255 nm and about 0.29 nm, which can be interpreted as a disturbed BCC-like arrangement, and Tb atoms mainly at a distance of about 0.307 nm. The number $Z_{FeFe} + Z_{FeTb}$ of atoms in the first coordination shell of an Fe atom decreases with increasing

Tb content from 13.7 for $Fe_{90}Tb_{10}$ to 10.4 for $Fe_{68}Tb_{32}$ and to 8.6 for $Fe_{50}Tb_{50}$.

For FeTb alloys a compound formation tendency has been postulated by some authors (e.g.[3,4]). This can be decided from the ratio of the partial coordination numbers of the next neighbours, which may be different to the macroscopic ratio of the contributing elements. In the case of compound formation in the first coordination shell of Fe more Tb atoms can be found than one would expect from the atomic fraction of Tb in the alloy as a whole. Actually, we also find a surplus of Tb atoms between 0.7 and 1.1 for all alloys investigated up to $Fe_{68}Tb_{32}$ (see table 4).

This is a smaller amount than found by other authors, because we find systematically larger FeFe coordination numbers and smaller FeTb coordination numbers. The reason for this is the BCC-like shape of the partial FeFe RDFs as discussed above. This can be seen by comparing the coordination numbers for $Fe_{68}Tb_{32}$ from the Gaussian fit with the formerly presented results. Nevertheless, the Tb surplus is significant for all the alloys up to $Fe_{68}Tb_{32}$, indicating compound formation in the alloys where the Fe atoms are preferentially surrounded by Tb atoms and vice versa, although we find a BCC Fe-like surrounding in the FeFe RDFs. Actually, as has been shown, such a BCC-like surrounding can also be constructed by superposing the FeFe surroundings of the crystalline FeTb structures. So, there is no contradiction between these two results, and in particular no segregation tendency for the Fe atoms in the Fe-rich alloys can be concluded.

A different result can be found for $Fe_{50}Tb_{50}$: here we find 0.5 Tb atoms less in the Fe surroundings compared to what a statistical distribution would predict, meaning a segregation tendency for this alloy.

4. Summary and interpretation

It has been shown that thin films of FeTb alloys prepared by RF sputtering are amorphous for a Tb content of 10 at.% or more. They contain approximately 2 at.% Ar due to the sputtering process. The films are metastable at room temperature, oxidation can be prevented by coating the films with a sputtered Al layer of about 5 nm thickness. Electron diffraction in a conventional electron microscope with 300 keV electrons is a suitable method to investigate the atomic arrangement of these films. It is possible to obtain large scattering lengths, meaning a high resolution in the PDFs calculated from the diffraction intensities. Measuring the PDF of a known crystalline structure, here BCC Fe, it is possible to correct the scattering intensities for inelastic- and multiple-scattering contributions for the specific experimental conditions used.

It has been shown that the short-range order of the measured PDFs of Fe-rich alloys can be described quantitatively as an arrangement of crystalline-like FeTb structures with various concentrations and structures by superposing PDFs of these structures and of crystalline BCC Fe and HCP Tb. The short-range order of amorphous $Fe_{50}Tb_{50}$ cannot be described correctly with this multicrystalline model. To obtain FeFe, FeTb and TbTb neighbour distances and coordination numbers for this special alloy, three Gaussians have been fitted.

The partial RDFs calculated for the Fe-rich alloys show more complicated structures for the FeFe and FeTb coordination than a description with Gaussian-shaped curves, which is normally used. The FeFe RDFs show an asymmetric shape with two FeFe distances at about 0.255 and 0.29 nm for all Fe-rich alloys. The FeTb-PDFs show a main maximum between 0.30 and 0.31 nm. These next-neighbour distances are in general agreement with results from other authors, but due to the described bcc-like FeFe coordination a stronger overlap between the partial FeFe and FeTb RDFs occurs, leading to systematically larger FeFe coordination numbers and smaller FeTb coordination numbers, respectively, which seem to be more accurate.

Nevertheless, the often postulated compound formation for the Fe-rich alloys could also be confirmed from our data. We find a surplus of Tb atoms in the coordination shell of Fe, compared to a statistical distribution. For $Fe_{50}Tb_{50}$ we find 0.5 Tb atoms less than a statistical distribution predicts, meaning a segregation tendency in this alloy.

From this we conclude that compound formation occurs in a composition range where the short-range order of the alloys can be described with our MC model as locally optimized crystalline-like FeTb structures. This tendency is *not* disturbed by a BCC-like FeFe coordination, because in crystalline FeTb structures FeFe distances similiar to the FeFe distances in BCC Fe exist, so that they match the Fe-BCC structure. On the contrary, no crystalline FeTb structure exists with a TbTb distance similiar to that in the HCP Tb structure that dominates the $Fe_{50}Tb_{50}$ amorphous alloy. Therefore no locally stoichiometric optimized structure containing Fe atoms can be formed in this alloy, the Fe atoms seem to be distributed more randomly between HCP Tb-like ordered regions. This structure may well be described in terms of a dense random packing (DRP) model.

Acknowledgments

This work has been supported by the EC Commission under contract No SC1*/0106-C-CCMB and by the Friedrich-Ebert-Foundation, Bonn, Federal Republic of Germany.

References

[1] Cargill G S 1974 *AIP Conf. Proc.* **18** 631
[2] Fukuda K, Katayama S, Katayama T, Nukui A and Makisima A 1986 *Japan. J. Appl. Phys.* **25** 1640
[3] Utz R, Brunsch A, Lamparter P and Steeb S 1989 *Z. Naturf.* a **44** 1201
[4] Matsubara E, Waseda Y, Kato Y and Takayama S 1990 *Mater. Trans. Japan. Inst. Met.* **31** 739
[5] Suzuki K, Misawa M, Fukunaga T and Hayashi N 1980 *Proc. Metal. Glasses: Sci. Technol. (Budapest)* **1** 327
[6] Williams D E G 1982 *Phys. Status Solidi* a **73** 539
[7] Hayes T M and Wright A C 1982 *The Structure of Non-crystalline Materials* ed Gaskell, Parker and Davis (London: Taylor & Francis) p 108
[8] Suzuki K 1983 *Amorphous Metallic Alloys* ed F E Luborsky (London: Butterworth) p 78
[9] Lines M E 1983 *J. Magn. Magn. Mater.* **36** 1
[10] Tewes M, Zweck J and Hoffmann H 1991 *J. Magn. Magn. Mater.* **95** 43
[11] Steeb S 1968 *Springer Tracts in Modern Physics* vol 47 (Berlin: Springer) p 2
[12] Lorch E 1969 *J. Phys. C: Solid State Phys.* **2** 229
[13] Robinson C J, Samant M G and Marinero E E 1989 *Appl. Phys.* A **49** 619
[14] Anstis G R, Liu Z and Lake M 1988 *Ultramicroscopy* **26** 65–70
[15] Nandra S S and Grundy P J 1977 *J. Phys. F: Met. Phys.* **7** 207
[16] O'Leary W P 1975 *J. Phys. F: Met. Phys.* **5** 175
[17] Hatta S, Mizoguchi T and Watanabe N 1985 *Proc. 5th Conf. on Rapidly Quenched Metals (RQ5) (Würzburg, 1985)* ed S Steeb and H Warlimont (Amsterdam: North-Holland) p 589
[18] Orlowa I G, Eliseev A A, Chuprikov G E and Rukk F 1977 *Russ. J. Inorg. Chem.* **22** 1387
[19] Aptekar L I 1980 *Proc. Metal. Glasses: Sci. Technol. (Budapest)* **1** 253
[20] Gaskell P H 1979 *J. Phys. C: Solid State Phys.* **12** 4337